IEEE Access
Multidisciplinary | Rapid Review | Open Access Journal

Received 16 February 2023, accepted 15 March 2023, date of publication 20 March 2023, date of current version 28 March 2023.

Digital Object Identifier 10.1109/ACCESS.2023.3258971

RESEARCH ARTICLE

Microwave Frequency Dividers With Reconfigurable Fractional 2/*N* and 3/*N* Division Ratios

HAO CHEN, (Member, IEEE), MINGTONG LIU, AOQI LI, AND ERWIN H. W. CHAN, (Senior Member, IEEE)
Faculty of Science and Technology, Charles Darwin University, Darwin, NT 0810, Australia
Corresponding author: Erwin H. W. Chan (erwin.chan@cdu.edu.au)

ABSTRACT Two microwave photonic signal processing structures, which are capable to realise microwave frequency division with a tunable integer or non-integer division ratio, are presented. They are based on applying an RF signal into a Mach Zehnder modulator, which is biased to generate a carrier-suppressed double sideband (DSB) or single sideband (SSB) optical signal. The carrier-suppressed DSB optical signal consists of the upper and lower 1st order sidebands with a separation of two times the input RF signal frequency. The carrier of the SSB optical signal is suppressed by a fibre Bragg grating (FBG) connected to the modulator output. Hence the FBG output consists of the upper 1st order and lower 2nd order sidebands with a separation of three times the input RF signal frequency. The carrier-suppressed DSB or SSB optical signal is injected into a semiconductor laser. The semiconductor laser is oscillated in the period-one state that generates a number of equally spaced frequency components, which are frequency locked by the injection light wave. Beating of these optical frequency components at the photodetector produces an RF signal with a frequency of 2/*N* or 3/*N* times the input RF signal frequency where *N* can be between 3 and 6. Hence the 2/*N* frequency divider can realise 2/3, 1/2, 2/5 and 1/3 frequency division operation, and the 3/*N* frequency divider can realise 3/4, 3/5 and 1/2 frequency division operation. The proposed 2/*N* and 3/*N* frequency dividers have a very simple structure compared to the reported photonics-based microwave frequency divider that can realise both integer and non-integer frequency divisions. The frequency division ratio can be tuned by simply adjusting the forward bias current of the semiconductor laser subject to optical injection. Experimental results demonstrate the two proposed structures can realise microwave frequency division with a tunable integer and non-integer division ratio for different input RF signal frequencies of 10 to 18 GHz, and over 60 dB output signal-to-noise ratio performance. More than 27 dB suppression in the unwanted frequency components around the frequency divided signal is also demonstrated.

INDEX TERMS Semiconductor laser, optical injection, periodic oscillation, frequency division.

I. INTRODUCTION

Microwave frequency dividers are widely used in radar, communication, military, test and measurement systems. Recently there are several reports on microwave frequency dividers implemented using microwave photonic technologies [1], [2], [3], [4], [5], [6], [7], [8]. This is because photonics offers the advantages of wide bandwidth, immunity to electromagnetic interference, reconfigurability and integrability [9], [10], [11]. Photonics-based microwave frequency dividers can be implemented using the regenerative technique or the injection locking technique, which were originally developed for electronic frequency dividers many decades ago [12]. They can also be implemented using optical approaches such as utilising the nonlinear effect in a semiconductor optical amplifier or a semiconductor laser.

Photonics-based microwave frequency dividers with a tunable frequency division ratio have been demonstrated via the

The associate editor coordinating the review of this manuscript and approving it for publication was Wen Chen.

regenerative technique [1], [2], the injection locking technique [4], [5] and the optically injected semiconductor laser technique [8]. Almost all of them are focused on realising frequency division with a tunable integer frequency division ratio so that the frequency of the output RF signal is 1/N times the input RF signal frequency, where N is an integer. Fractional or non-integer frequency dividers generate an output RF signal with the same frequency as the input RF signal frequency divided by a non-integer. Examples of non-integer frequency dividers are the 2/3 and 2/5 frequency dividers because their frequency division ratios are 1/1.5 and 1/2.5 respectively. Non-integer frequency dividers are required in wireless communications especially for multifunction or multiservice applications [13]. They are also employed in a frequency synthesizer to improve the frequency range and resolution of the generated signal [14]. Frequency dividers with a non-integer frequency division ratio can be realised by using the combination of frequency dividers and multipliers. However, this increases the system complexity, size and cost. To the best of our knowledge, until now there is only one reported microwave photonic structure that can realise microwave frequency division with both integer (1/2 and 1/3) and non-integer (2/3 and 2/5) division ratios [2]. This frequency divider is constructed using the regenerative technique through an optoelectronic oscillator (OEO) loop, which involves a number of electrical components including an electrical phase shifter, electrical amplifiers and electrical couplers. It also requires two dual-parallel Mach Zehnder modulators (DP-MZMs) connected in series. Tuning the frequency division ratio or changing the input RF signal frequency requires adjusting the modulator bias voltages, and the gain and phase of the signal travelling in an OEO loop to satisfy the gain and phase condition. It is highly desirable for a photonics-based microwave frequency divider to have a simple and compact structure, and to be capable of realising frequency division with both integer and non-integer division ratios that can be tuned easily. Until now, such a tunable photonics-based microwave frequency divider does not exist.

Two photonics-based integer and non-integer microwave frequency dividers are presented. They are based on the optically injected semiconductor laser technique. A number of microwave photonic signal processors such as microwave signal generators [15] and microwave frequency converters and multipliers [16] have been developed using this technique. The first structure uses a null-biased Mach Zehnder modulator (MZM) to generate a carrier-suppressed double sideband (CS-DSB) optical signal, which is injected into a semiconductor laser for realising 2/N frequency division. The second structure uses a dual-drive MZM (DD-MZM) and a fibre Bragg grating (FBG) to generate an optical signal with the carrier and the lower 1st order sideband being suppressed. This optical signal is injected into a semiconductor laser for realising 3/N frequency division. Only the semiconductor laser forward bias current needs to be adjusted to tune the frequency division ratio. Experimental results are presented which demonstrate integer (1/2 and 1/3) and non-integer (2/3 and 2/5) frequency division using the 2/N frequency divider, and integer (1/2) and non-integer (3/4 and 3/5) frequency division using the 3/N frequency divider, for an input RF signal in a 10 to 18 GHz frequency range. Large unwanted frequency component suppression of over 27 dB around the frequency divided signal and high signal-to-noise ratio (SNR) of over 60 dB in a 100 kHz noise bandwidth are also demonstrated.

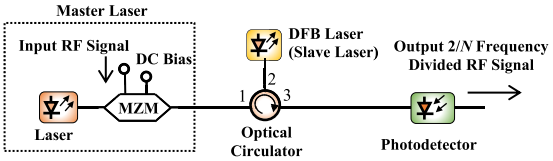

FIGURE 1. Photonics-based 2/N microwave frequency divider topology.

II. FREQUENCY DIVIDER TOPOLOGIES AND OPERATION PRINCIPLE

A. 2/N MICROWAVE FREQUENCY DIVIDER

Fig. 1 shows the structure of the proposed 2/N microwave frequency divider. As shown, it is basically a microwave photonic link with an optical circulator and a DFB laser inserted at the output of an optical modulator. The optical modulator is a null-biased MZM driven by an RF signal whose frequency needs to be divided. It is well known that the output of a null-biased MZM is a CS-DSB optical signal, which consists of upper and lower first ($\pm 1^{st}$) order RF modulation sidebands with the optical carrier being suppressed. Therefore, the electric field at the modulator output can be written as

$$E_{MZM}(t) = \sqrt{t_{ff}} E_{in} e^{j\omega_c t} \left[-J_1(\beta_{RF}) e^{-j\omega_{RF} t} + J_1(\beta_{RF}) e^{j\omega_{RF} t} \right] \quad (1)$$

where t_{ff} is the MZM insertion loss, E_{in} and $\omega_c = 2\pi f_c$ are the electric field amplitude and the angular frequency of the continuous wave (CW) light into the MZM, $J_n(x)$ is the Bessel function of n^{th} order of the first kind, $\omega_{RF} = 2\pi f_{RF}$ is the angular frequency of the input RF signal, $\beta_{RF} = \pi V_{RF}/V_\pi$ is the modulation index, V_{RF} is the input RF signal amplitude and V_π is the MZM RF port switching voltage. The laser source and the null-biased MZM form a master laser (ML). The two $\pm 1^{st}$ order sidebands at the ML output are the injection light wave, which is injected into a slave laser (SL) via an optical circulator. The SL is a standard off-the-shelf DFB laser. The frequency of the light generated by the DFB laser without subject to optical injection is called the free running frequency and is between the two $\pm 1^{st}$ order sidebands of the injection light wave. The spectra of the injection light wave from the ML and the free running SL are shown in Fig. 2(a). The figure shows the separation of the two injection light wave frequency components is $2f_{RF}$. The

SL forward bias current can be designed to alter the SL free running frequency and power. This consequently changes the detuning frequency f_i, which is defined as the SL free running frequency offset from the ML, and the injection strength ξ, which is defined as the square root of the power ratio between the light wave from the ML and the free running SL [17], [18]. Since the ML consists of two optical frequency components, there are two sets of detuning frequency and injection strength associated with a SL forward bias current. By designing the SL forward bias current so that the SL free running frequency is close to the -1^{st} order sideband at f_c-f_{RF} of the injection light wave as shown in Fig. 2(a), the SL mainly interacts with the -1^{st} order sideband, which results in the SL oscillated in the period-one (P1) state [15], [16]. When the SL oscillates in the P1 state, the output of the SL consists of the regenerated injection light wave, a fundamental oscillation at f_{osc} and its harmonics at $f_{osc}\pm nf_o$ where f_o is a fundamental frequency [19]. The frequencies of the fundamental oscillation and the harmonics can be controlled by adjusting the SL forward bias current, which alters the detuning frequencies and the injection strengths. Fig. 2(b) shows an example of the SL output optical spectrum where the SL forward bias current is adjusted to generate a fundamental oscillation at f_c-$f_{RF}/3$ and a harmonic at f_c+$f_{RF}/3$ between the two regenerated $\pm1^{st}$ order sidebands. Note that two adjacent optical frequency components shown in Fig. 2(b) have the same frequency separation of $f_o = 2f_{RF}/3$. The lower second (-2^{nd}) order harmonic and the upper third ($+3^{rd}$) order harmonic of the fundamental oscillation are aligned with the regenerated -1^{st} and $+1^{st}$ order sidebands respectively. Under this situation, the SL output is stable as it is frequency locked by the injection light wave. Beating of the optical frequency components with $2f_{RF}/3$ separation at the photodetector generates an RF signal at $2f_{RF}/3$. This shows the system shown in Fig. 1 can generate an RF signal with a frequency of 2/3 times the input RF signal frequency. Hence it can realise 2/3 microwave frequency division.

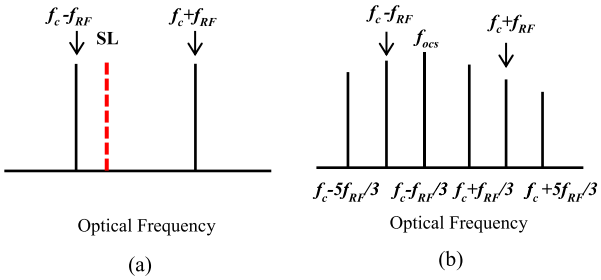

FIGURE 2. (a) Spectra of the master laser (black lines) and the free running slave laser (red dashed line). (b) Slave laser output optical spectrum for realising 2/3 microwave frequency division.

The SL forward bias current can be adjusted to generate n number of equally spaced optical frequency components between the two regenerated $\pm1^{st}$ order sidebands at the SL output. When n is an even integer, the SL output electric field can be written as

$$E_{o,SL,even}(t) = \sqrt{t_{ff}}E_{in}e^{j\omega_c t} \times \sum_{m=0}^{\infty}\left(A_{k_1(m)}e^{j(k_1(m)\omega_{RF}t+\theta_{k_1(m)})} + A_{-k_1(m)}e^{j(-k_1(m)\omega_{RF}t+\theta_{-k_1(m)})}\right) \quad (2)$$

where $A_{\pm k1(m)}$ and $\theta_{\pm k1(m)}$ are the amplitude and phase of the optical frequency component at $f_c \pm k_1(m) \times f_{RF}$, and $k_1(m) = (2m+1)/(n+1)$. When n is an odd integer, the SL output electric field can be written as

$$E_{o,SL,odd}(t) = \sqrt{t_{ff}}E_{in}e^{j\omega_c t} \times \left(A_0e^{j\theta_0} + \sum_{m=0}^{\infty}\left(A_{k_2(m)}e^{j(k_2(m)\omega_{RF}t+\theta_{k_2(m)})} + A_{-k_2(m)}e^{j(-k_2(m)\omega_{RF}t+\theta_{-k_2(m)})}\right)\right) \quad (3)$$

where $A_{\pm k2(m)}$ and $\theta_{\pm k2(m)}$ are the amplitude and phase of the optical frequency component at $f_c \pm k_2(m) \times f_{RF}$, and $k_2(m) = (2m+2)/(n+1)$. Since the separation of the two $\pm1^{st}$ order sidebands is $2f_{RF}$ and there are n number of equally spaced optical frequency components between the two regenerated $\pm1^{st}$ order sidebands at the SL output, the separation between two adjacent optical frequency components is $2f_{RF}/(n+1)$. Beating of these optical frequency components at the photodetector generates an RF signal with a frequency of $2/(n+1)$ times the input RF signal frequency f_{RF}. This shows the proposed structure shown in Fig. 1 can realise $2/N$ frequency division operation, where N is an integer. The experimental results presented in Section IV show N can be between 3 to 6.

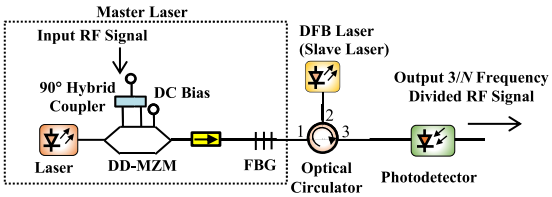

FIGURE 3. Photonics-based 3/N microwave frequency divider topology.

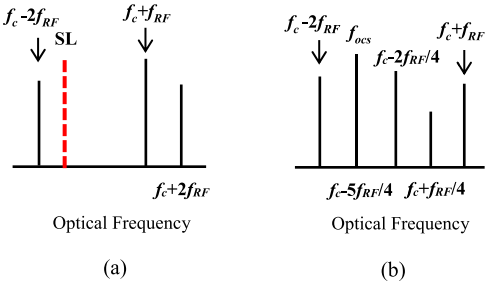

FIGURE 4. (a) Spectra of the master laser (black lines) and the free running slave laser (red dashed line). (b) Slave laser output optical spectrum for realising 3/4 microwave frequency division.

B. 3/N MICROWAVE FREQUENCY DIVIDER

A 3/N frequency divider can be implemented using the same operation principle as the 2/N frequency divider. Here the ML needs to generate two optical frequency components with a frequency separation of $3f_{RF}$. This can be achieved by using a DD-MZM with a 90° hybrid coupler connected to the two input RF ports of the modulator and a FBG connected to the DD-MZM output as shown in Fig. 3. The DD-MZM is biased at the quadrature point. The output of the DD-MZM is a single-sideband (SSB) RF modulated optical signal, which consists of an optical carrier and sidebands where the -1^{st} order sideband is being suppressed. A FBG with a centre wavelength the same as the laser source wavelength, is connected to the SSB modulator output to suppress the optical carrier. The optical isolator between the DD-MZM and the FBG is used to prevent the optical carrier reflected by the FBG into the DD-MZM. The output of the FBG consists of the $+1^{st}$ order sideband and $\pm 2^{nd}$ order sidebands as shown in Fig. 4(a). The electric field at the FBG output can be written as

$$E_{o,FBG}(t) = \frac{1}{2}\sqrt{t_{ff}}E_{in}e^{j\omega_c t}\Big[J_2(\beta_{RF})(1-j)\,e^{-j2\omega_{RF}t} + 2J_1(\beta_{RF})\,e^{j\omega_{RF}t} + J_2(\beta_{RF})(1-j)\,e^{j2\omega_{RF}t}\Big] \tag{4}$$

As shown in Fig. 4(a), the $+1^{st}$ and -2^{nd} order sidebands from the ML have a frequency separation of $3f_{RF}$. The output of the ML is injected into the SL via an optical circulator. The SL free running frequency is between the -2^{nd} order and the $+1^{st}$ order sidebands. As in the case of the 2/N frequency divider, the SL forward bias current can be adjusted so that the SL is oscillated in the P1 state, which can generate different numbers of equally spaced optical frequency components between the regenerated -2^{nd} order and $+1^{st}$ order sidebands at the SL output. When there are $n>1$ number of equally spaced optical frequency components between the two regenerated sidebands, the electric field at the output of the SL can be written as

$$E_{o,SL}(t) = \frac{1}{2}\sqrt{t_{ff}}E_{in}e^{j\omega_c t}\sum_{m=0}^{n+1}A_{k_3(m)}e^{j\left(k_3(m)\omega_{RF}t+\theta_{k_3(m)}\right)} \tag{5}$$

where $A_{k3(m)}$ and $\theta_{k3(m)}$ are the amplitude and the phase of the optical frequency component at $f_c \pm k_3(m)\times f_{RF}$, and $k_3(m) = (n+1-3m)/(n+1)$. Note that, for simplicity, only the frequency components within and including the -2^{nd} order and $+1^{st}$ order sidebands are considered in (5). Since the separation of the two regenerated -2^{nd} order and $+1^{st}$ order sidebands is $3f_{RF}$ and there are n number of equally spaced optical frequency components between the two regenerated sidebands, the separation between two adjacent optical frequency components at the SL output is $3f_{RF}/(n+1)$. Beating of these optical frequency components at the photodetector generates an RF signal with a frequency of $3/(n+1)$ times the input RF signal frequency f_{RF}. This shows the proposed structure shown in Fig. 3 can realise 3/N frequency division.

As an example, Fig. 4(b) shows the SL output spectrum when the SL forward bias current is adjusted to generate three equally spaced frequency components, i.e. the fundamental oscillation at $f_{osc} = f_c - 5f_{RF}/4$ and its 2^{nd} and 3^{rd} order harmonics at $f_c - 2f_{RF}/4$ and $f_c + f_{RF}/4$ respectively, between the regenerated -2^{nd} order and $+1^{st}$ order sidebands. In this case, the separation between two adjacent optical frequency components is $3f_{RF}/4$. Beating of these optical frequency components at the photodetector generates a microwave signal at $3f_{RF}/4$.

III. SIMULATION RESULTS AND DISCUSSION

The above analysis assumes the 2/N and 3/N frequency dividers are operated under an ideal situation. In practice, there is loss imbalance in the two arms of an MZM. Therefore, the optical carrier cannot be fully suppressed at the output of a null-biased MZM. With the inclusion of the loss imbalance in the two arms of the MZM in the 2/N frequency divider analysis, the electric field of the injection light wave becomes

$$E_{o,MZM}(t) = E_{in}e^{j\omega_c t}\sqrt{t_{ff}}\Big[(1-\gamma)J_2(\beta_{RF})\,e^{-j2\omega_{RF}t} - (1+\gamma)J_1(\beta_{RF})\,e^{-j\omega_{RF}t} + (1-\gamma)J_0(\beta_{RF}) + (1+\gamma)J_1(\beta_{RF})\,e^{j\omega_{RF}t} + (1-\gamma)J_2(\beta_{RF})\,e^{j2\omega_{RF}t}\Big] \tag{6}$$

where $\gamma = (\varepsilon^{1/2}-1)/(\varepsilon^{1/2}+1)$ and ε is the MZM extinction ratio. (6) shows, in addition to the two $\pm 1^{st}$ order sidebands, the null-biased MZM output also has a residual carrier and two $\pm 2^{nd}$ order sidebands. The effect of the two $\pm 2^{nd}$ order sidebands on the SL nonlinear dynamic can be neglected as they have small amplitudes and are far away from the free running SL. On the other hand, the carrier, which is close to the free running SL, needs to be largely suppressed to avoid interaction with the SL. The power ratio of the $\pm 1^{st}$ order sidebands to the residual carrier can be obtained using (6). It was plotted against the MZM extinction ratio for different modulation indexes in Fig. 5. As shown, for an MZM having an extinction ratio of 26 dB and 30 dB, a modulation index of 0.9 and 0.6 is needed respectively, in order to ensure the residual carrier is 20 dB below the two $\pm 1^{st}$ order sidebands. Note that the injection light wave is regenerated at the SL output. Hence, it is important to ensure the residual carrier and the two $\pm 2^{nd}$ order sidebands have small amplitudes, not only to avoid them to interact with the SL but also to minimise these unwanted optical frequency components to be regenerated by the SL, which beat with the desired frequency components at the photodetector that produces unwanted electrical frequency components at the system output.

In the case of the 3/N frequency divider, the DD-MZM extinction ratio has little effect on the system performance. The amount of the optical carrier suppression is determined by the FBG stopband rejection level η. The amount of the unwanted -1^{st} order sideband suppression is determined by the 90° hybrid coupler phase imbalance. With the inclusion of

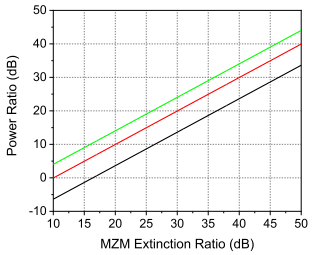

FIGURE 5. Power ratio of the ±1st order sidebands to the residual carrier versus the MZM extinction ratio for a modulation index of 0.3 (black line), 0.6 (red line) and 0.9 (green line), in the 2/*N* frequency divider.

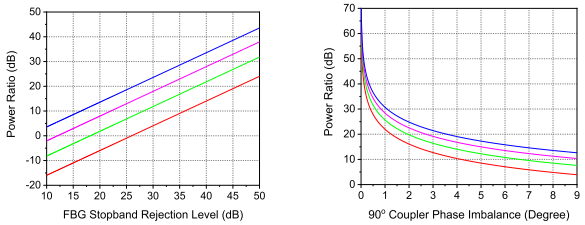

FIGURE 6. (a) Power ratio of the -2^{nd} order sideband to the residual carrier versus the FBG stopband rejection level, and (b) power ratio of the -2^{nd} order sideband to the unwanted -1^{st} order sideband versus the 90° hybrid coupler phase imbalance, for a modulation index of 0.6 (red line), 0.9 (green line), 1.2 (pink line) and 1.5 (blue line), in the 3/*N* frequency divider.

the FBG stopband rejection level and the 90° hybrid coupler phase imbalance in the 3/*N* frequency divider analysis, the electric field of the injection light wave becomes

$$\begin{aligned} &E_{o,FBG}(t) \\ &= \frac{1}{2}\sqrt{t_{ff}}E_{in}e^{j\omega_c t}\left[J_2(\beta_{RF})\,e^{-j2\omega_{RF}t}\left(1-e^{-j(2\varphi+\frac{\pi}{2})}\right)\right. \\ &\quad - J_1(\beta_{RF})\,e^{-j\omega_{RF}t}\left(1-e^{-j\varphi}\right)+\sqrt{\eta}J_0(\beta_{RF})(1-j) \\ &\quad + J_1(\beta_{RF})\,e^{j\omega_{RF}t}\left(1+e^{j\varphi}\right) \\ &\quad \left. + J_2(\beta_{RF})\,e^{j2\omega_{RF}t}\left(1-e^{j(2\varphi-\frac{\pi}{2})}\right)\right] \end{aligned} \tag{7}$$

where φ is the phase difference of the two 90° hybrid coupler output ports deviated from 90°. Under an ideal situation, both η and φ are 0, and hence (7) becomes (4). Since the residual carrier and the unwanted -1^{st} order sideband are close to the free running SL, they need to be largely suppressed to avoid interaction with the SL. Using (7), Fig. 6(a) shows, for an FBG with 38 dB stopband rejection level, the modulation index needs to be above 0.9 in order for the -2^{nd} order sideband to be more than 20 dB above the residual carrier. Fig. 6(b) shows, a modulation index of 1.2 is needed to ensure the -2^{nd} order sideband is more than 20 dB above the unwanted -1^{st} order sideband when the 90° hybrid coupler has a phase imbalance of 2.7°.

As can be seen from Fig. 1, the 2/*N* frequency divider does not involve electrical components. Both the MZM bandwidth and the optically injected semiconductor laser bandwidth can be 100 GHz [16], [20]. Hence 2/*N* frequency division operation can be realised beyond microwave and well into millimetre wave frequency. The 3/*N* frequency divider requires an FBG to remove the optical carrier and a 90° hybrid coupler to realise SSB modulation. FBGs with a narrow 3-dB reflection spectrum width of less than 10 GHz and a high stopband rejection level of around 40 dB are commercially available [21]. The upper operating frequency of the 3/*N* frequency divider is limited by the 90° hybrid coupler bandwidth. 90° hybrid couplers with a 4-40 GHz bandwidth and ±4° phase imbalance [22] can be used to implement the proposed 3/*N* frequency divider with an upper operating frequency of 40 GHz. Wider bandwidth 90° hybrid couplers are commercially available. However, their phase imbalance is larger than ±4° and hence a high modulation index, i.e. a high input RF signal power, is needed to ensure the unwanted -1^{st} order sideband is at least 15 dB below the -2^{nd} order sideband. Both 2/*N* and 3/*N* frequency dividers shown in Fig. 1 and 3 not only have simple structures but also have a tunable frequency division ratio. Only a single system parameter, i.e. the SL forward bias current, needs to be adjusted to obtain difference frequency division ratios. This is very simple compared to the reported 1/*N* frequency dividers based on the regenerative technique [1] and the injection locking technique [4]. Tuning the frequency division ratio of the regenerative based 1/*N* frequency divider requires adjusting the centre frequency and the passband width of an optical filter, and the gain of an erbium-doped fibre amplifier (EDFA) and the length of a variable delay line for the OEO loop to satisfy the gain and phase conditions [1].

It should be pointed out that the proposed 2/*N* frequency divider has the same structure as the reported 1/2 frequency divider [7]. However, they have different operation principles. For the proposed 2/*N* frequency divider, the MZM is biased at the null point to suppress the optical carrier. The SL is mainly interacted with the -1^{st} order sideband and is oscillated in the P1 state, which generates the fundamental oscillation and its harmonics. For the reported 1/2 frequency divider, the MZM is biased at the quadrature point. In this case, the SL interacts with both the -1^{st} order sideband and the optical carrier, and is oscillated in the period-two (P2) state. The proposed 2/*N* and 3/*N* frequency dividers have different structures, different operation principles and different performances compared to other reported optically injected semiconductor laser based frequency dividers. For example the frequency divider presented in [6] has a fixed 1/2 division ratio. It is implemented by a SL operated under direct modulation and is designed to oscillate at the P2 state. The frequency divider presented in [8] can only realise an integer 1/*N* frequency division. It is implemented by applying an RF signal to an optical phase modulator in the ML and the SL is designed to oscillate at the period-*N* state.

IV. EXPERIMENTAL RESULTS

An experiment was set up, similar to that shown in Fig. 1, to demonstrate the proposed 2/*N* frequency divider. The laser source was a tunable laser (Keysight N7711A). The CW light

generated by the tunable laser passed through a polarisation controller (PC) into an optical modulator. The optical modulator was a DD-MZM (Fujitsu FTM7937EZ200). It has an extinction ratio of around 26 dB and an RF port switching voltage of 3.3 V at 18 GHz. A 1-18 GHz 3-dB bandwidth 180° hybrid coupler was connected to the two modulator input RF ports. Hence the optical modulator behaved like the single-drive MZM shown in Fig. 1. An 18 GHz RF signal from a microwave signal generator was applied to the DD-MZM via the 180° hybrid coupler. The RF modulated optical signal at the DD-MZM output passed through a PC and routed from Port 1 to Port 2 of an optical circulator into a SL. The SL was a standard off-the-shelf DFB laser. A temperature controller (Newport 350B) and a laser diode driver (Newport 505B) were employed to control the DFB laser temperature and to provide a forward bias current to the DFB laser respectively. When the DFB was operating at 25 °C, it generated CW light with a frequency of 193.517 THz and 193.468 THz for a 10 mA and 80 mA forward bias current respectively. Port 3 of the optical circulator was connected to an EDFA followed by a 0.5 nm 3-dB bandwidth optical filter, which were used to compensate for the system loss and to suppress the amplified spontaneous emission (ASE) noise. The system output optical signal was detected by a photodetector (Discovery Semiconductor DSC30S), which had a 3-dB bandwidth of around 23 GHz.

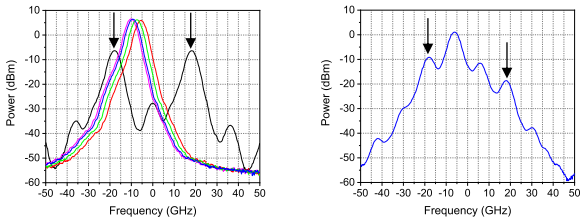

FIGURE 7. (a) Optical spectrum of the ML when the null-biased DD-MZM is driven by an 18 GHz RF signal (black line), and optical spectra of the free running SL for realising 2/3 (red line), 2/4 (green line), 2/5 (blue line) and 2/6 (pink line) frequency division. The frequency of the residual carrier from the ML is normalised to 0 Hz. (b) SL output optical spectrum when the SL forward bias current is adjusted to realise 2/3 frequency division.

The frequency of the CW light generated by the tunable laser was set to be 193.501 THz, which is close to the DFB laser free running frequency. The DD-MZM was biased at the null point to generate a CS-DSB optical signal with an optical spectrum shown by the black line in Fig. 7(a). The arrows in Fig. 7(a) indicate the $\pm 1^{st}$ order sidebands of the CS-DSB optical signal. It can be seen from the figure that the optical carrier is more than 21 dB below the two 1^{st} order sidebands. The power ratio of the 1^{st} and 3^{rd} order sidebands was found to be 29 dB. Since the 1^{st} and 3^{rd} order sideband powers are proportional to $J_1(\beta_{RF})^2$ and $J_3(\beta_{RF})^2$ respectively, the modulation index β_{RF} is 0.91. The DFB laser temperature was fixed at 25 °C and its forward bias current was increased to 47.7 mA to obtain two frequency components with a separation of 12 GHz between the two regenerated 1^{st} order sidebands at ±18 GHz away from the optical carrier. The two frequency components are the fundamental oscillation and its 2^{nd} order harmonic generated by the SL P1 nonlinear dynamic. The SL output optical spectrum was measured at Port 3 of the optical circulator and is shown in Fig. 7(b). The arrows in the figure indicate the $\pm 1^{st}$ order sidebands regenerated by the SL. The free running spectrum of the SL operating at 47.7 mA forward bias current is shown by the red line in Fig. 7(a). The detuning frequencies and the injection strengths can be obtained from the frequencies and the powers of the free running SL and the $\pm 1^{st}$ order sidebands of the injection light wave. The two sets of detuning frequencies and injection strengths were found to be $(f_{i1}, \xi_1) = (12.479\ \text{GHz}, 0.243)$ and $(f_{i2}, \xi_2) = (-23.715\ \text{GHz}, 0.243)$.

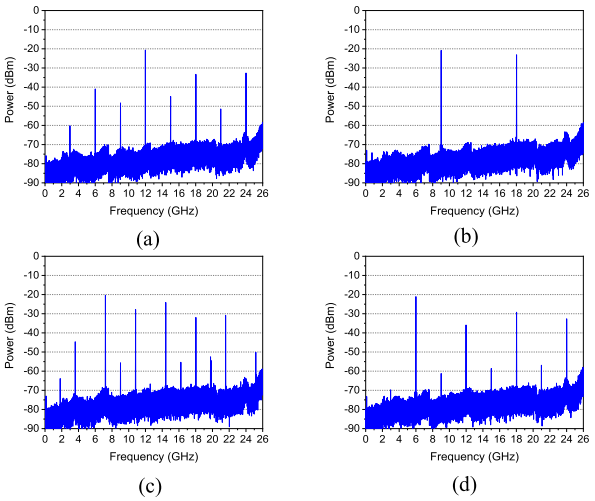

FIGURE 8. System output electrical spectra when the SL forward bias current is (a) 47.7 mA, (b) 50.2 mA, (c) 52.8 mA and (d) 53.9 mA.

Fig. 8(a) shows the system output electrical spectrum measured on an electrical signal analyser (ESA) connected to the photodetector output, when the SL forward bias current was 47.7 mA. As shown, a 12 GHz frequency component is generated at the system output. This verifies the proposed structure can realise 2/3 frequency division operation since the input RF signal frequency is 18 GHz. Note from Fig. 8(a) that, as with most reported photonics-based frequency dividers [1], [2], [3], [4], [5], a number of unwanted frequency components are present at the 2/3 frequency divider output. They are due to the loss imbalance in the two arms of the DD-MZM causing limited optical carrier suppression at the null-biased DD-MZM output. When the residual carrier is injected into the SL, the SL not only regenerates the residual carrier but also generates additional unwanted optical frequency components due to the SL nonlinearity. To investigate the effect of the residual carrier on the 2/3 frequency divider output, a Fourier domain optical processor (FD-OP) (Finisar WaveShaper WS-04000A) was connected to the output of the null-biased DD-MZM. Fig. 9(a) and 9(b) show the 2/3 frequency divider output electrical spectra when

the FD-OP was programmed to pass and to suppress the residual carrier, which results in the residual carrier being 21 dB and 43 dB below the two ±1st order sidebands respectively. The measurements indicate that, by using an FD-OP to suppress the residual carrier to be 43 dB below the two $\pm 1^{st}$ order sidebands, all the unwanted frequency components up to the 2^{nd} order harmonic of the 2/3 frequency divided signal are more than 27 dB below the 2/3 frequency divided signal at 12 GHz. This shows it is important to suppress the optical carrier in the injection light wave as much as possible to minimise the unwanted frequency components present at the system output. In practice, a high extinction ratio MZM [23] or a narrow bandwidth and high stopband rejection FBG [21] centred at the laser source wavelength connected to the modulator output can be used to largely suppress the optical carrier. The unwanted frequency component at 24 GHz shown in Fig. 9 is the 2^{nd} order harmonic of the frequency divided signal. It can be suppressed by using an optical filter to select the two high-amplitude optical frequency components at −18 GHz and −6 GHz shown in Fig. 7(b), and filter out the other optical frequency components generated by the SL. Over 40 dB harmonic suppression has been demonstrated using an optical filter in an optically injected semiconductor laser based 1/2 frequency divider [24].

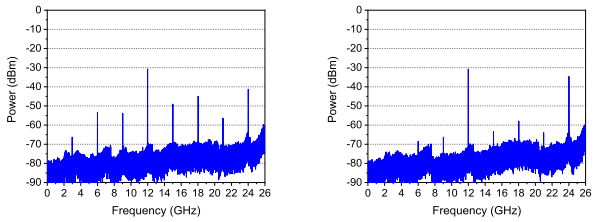

FIGURE 9. 2/3 frequency divider output electrical spectra when the FD-OP was programmed (a) to pass and (b) to suppress the residual carrier from the null-biased DD-MZM.

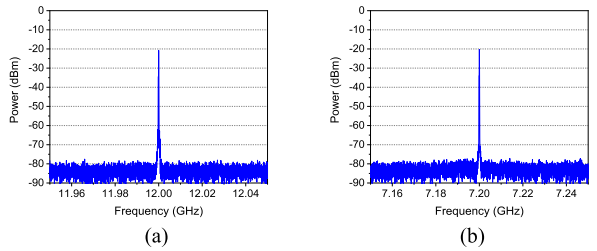

FIGURE 10. Output electrical spectra of the proposed 2/*N* frequency divider measured in a 100 MHz span when the SL forward bias current is adjusted to realise (a) 2/3 and (b) 2/5 frequency division. The ESA resolution bandwidth is 100 kHz and the ESA video bandwidth is 10 kHz.

Including the FD-OP in the setup to suppress the residual carrier increases the system complexity and loss. Hence, for simplicity, the FD-OP was removed in the subsequent 2/*N* frequency divider experiments. The SL forward bias current was increased from 47.7 mA to 50.2 mA, 52.8 mA and

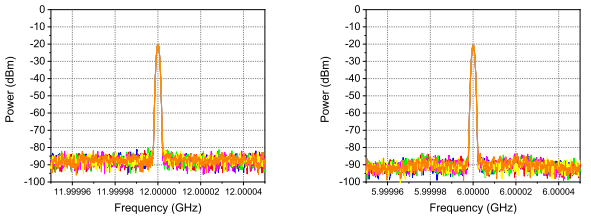

FIGURE 11. Proposed 2/*N* frequency divider output electrical spectra measured every two minutes in a measurement period of 10 minutes, when the SL forward bias current is adjusted to realise (a) 2/3 and (b) 2/6 frequency division. The ESA resolution bandwidth is 1 kHz and the ESA video bandwidth is 100 Hz.

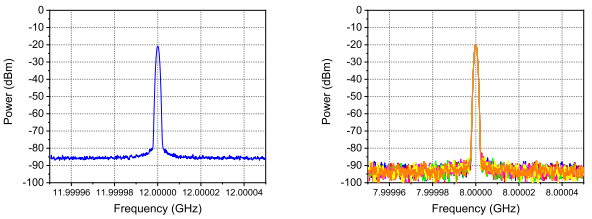

FIGURE 12. Proposed 2/3 frequency divider output electrical spectra (a) measured using the max-hold trace mode for an input RF signal frequency of 18 GHz and (b) measured every two minutes in a measurement period of 10 minutes for an input RF signal frequency of 12 GHz.

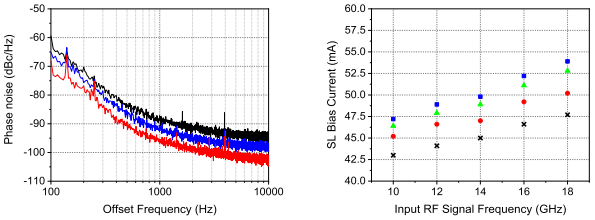

FIGURE 13. (a) Phase noise spectrum of the input 18 GHz microwave signal from the microwave signal generator (black) and the 2/3 and 2/6 frequency divided signals at 12 GHz (blue) and 6 GHz (red) respectively. (b) SL forward bias current required to realise 2/3 (black cross), 2/4 (red dot), 2/5 (green triangle) and 2/6 (blue square) frequency division versus the system input RF signal frequency.

53.9 mA so that the number of equally spaced optical frequency components between the two regenerated $\pm 1^{st}$ order sidebands at the SL output was increased from 2 to 3, 4 and 5 respectively. The corresponding system output electrical spectra are shown in Fig. 8(b)-8(d). As can be seen from Fig. 8, a frequency component at 12 GHz, 9 GHz, 7.2 GHz and 6 GHz was generated when an 18 GHz RF signal was injected into the proposed structure. This demonstrates the frequency division ratio of 2/3, 2/4, 2/5 and 2/6 can be tuned by simply adjusting the SL forward bias current. The experimental results show a high frequency division ratio requires a high SL forward bias current. It was found that a stable frequency divided signal could not be obtained when the SL forward bias current increased to above 55 mA while the

input RF signal frequency was fixed at 18 GHz. This could be due to the frequency difference between the ML and the free running SL is very small at this current level, which can be seen in Fig. 7(a). Hence the frequency division ratio is limited to 2/6. Fig. 10(a) and 10(b) show the 2/3 and 2/5 frequency divider output electrical spectra measured in a 100 MHz span around the frequency divided signal. The figures show the 2/*N* frequency divider has over 60 dB SNR in a 100 kHz noise bandwidth. The 2/3 and 2/6 frequency divider output electrical spectra were measured in a 100 kHz span around the frequency divided signal for every two minutes in a 10-minute measurement period. They are shown in Fig. 11(a) and 11(b). Fig. 12(a) shows the 2/3 frequency divider output obtained using the max-hold function in the ESA for 10 minutes. The 2/3 frequency divider stability measurement shown in Fig. 11(a) was repeated for an input RF signal frequency of 12 GHz. The corresponding 2/3 frequency divider output electrical spectra are shown in Fig. 12(b). The measurements shown in Fig. 11 and Fig. 12 reveal that the output of the 2/*N* frequency divider is stable for different frequency division ratios and different input RF signal frequencies. In the 10-minute measurement period, no frequency jitter was observed, and the amplitude of the frequency divided signal has less than 0.1 dB change. The phase noise of the 2/*N* frequency divider was measured on the ESA. Fig. 13(a) shows the phase noise spectra of the 2/3 and 2/6 frequency divided signals together with the phase noise spectrum of the input 18 GHz RF signal. It can be seen from the figure that, at 1-kHz frequency offset, the generated 2/3 and 2/6 frequency divided signals have 3.2 dB and 9 dB phase noise suppression compared with the input 18 GHz RF signal. This is consistent with the theoretical predicted phase noise improvement of $20\log_{10}(2/3)$=3.5 dB and $20\log_{10}(2/6)$=9.5 dB for the 2/3 and 2/6 frequency dividers respectively. The ability of the proposed 2/*N* frequency divider to generate a frequency divided signal with different division ratios for different input RF signal frequencies was investigated. Fig. 13(b) shows the SL forward bias current required to realise 2/3 to 2/6 frequency division for an RF signal with a frequency of 10 to 18 GHz into the system. It can be seen from the figure that the higher the input RF signal frequency and the frequency division ratio, the higher the SL forward bias current is needed. Note that the 2/6 frequency divider operated at 18 GHz input RF signal frequency only requires 53 mA SL forward bias current, which is well below the SL operating current of 80 mA given in the datasheet. Hence the 2/*N* frequency divider can be operated well beyond 18 GHz.

The 2/*N* frequency divider experimental setup was modified, similar to that shown in Fig. 3, to demonstrate the 3/*N* frequency division operation. This was done by replacing the 180° hybrid coupler with a 2-18 GHz 3-dB bandwidth 90° hybrid coupler and biasing the DD-MZM at the quadrature point to obtain a SSB optical signal. Since an FBG with a centre wavelength of around the DFB laser wavelength was not available, the optical carrier was suppressed by an FD-OP connected to the DD-MZM output. The black line

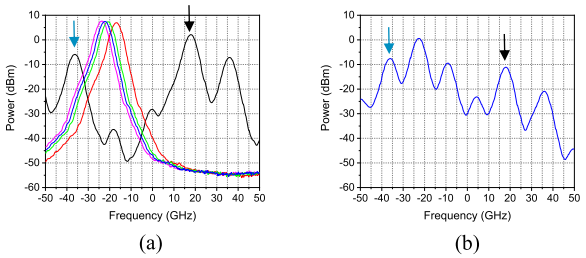

FIGURE 14. (a) Optical spectrum of the ML when the quadrature-biased DD-MZM operated as a SSB modulator is driven by an 18 GHz RF signal (black line). Optical spectra of the free running SL for realising 3/3 (red line), 3/4 (green line), 3/5 (blue line) and 3/6 (pink line) frequency division. The frequency of the residual carrier from the ML was normalised to 0 Hz. (b) SL output optical spectrum when the SL forward bias current is adjusted to realise 3/4 frequency division.

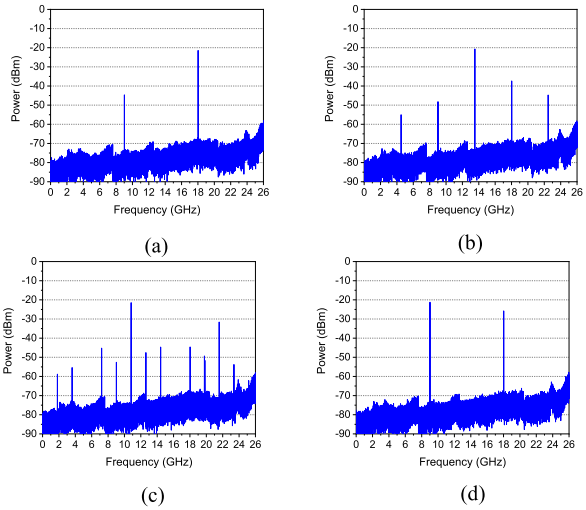

FIGURE 15. System output electrical spectra when the SL forward bias current is (a) 56.4 mA, (b) 61.3 mA, (c) 63 mA and (d) 64.7 mA.

in Fig. 14(a) shows the optical spectrum of the injection light wave when the DD-MZM is driven by an 18 GHz RF signal. The frequency of the residual carrier was normalised to 0 Hz. The modulation index, which can be estimated using the power ratio of the $+1^{st}$ and $+2^{nd}$ order sidebands, is 1.5. Fig. 14(a) shows the residual carrier and the -1^{st} order sideband are 22.4 dB and 30.5 dB respectively, below the -2^{nd} order sideband (blue arrow). The SL forward bias current was adjusted to 61.3 mA to obtain 3 equally spaced frequency components between the regenerated -2^{nd} order and $+1^{st}$ order (black arrow) sidebands at the SL output, as can be seen in the SL output spectrum shown in Fig. 14(b). The three optical frequency components are the fundamental oscillation and its 2^{nd} and 3^{rd} order harmonics. The corresponding SL free running spectrum is shown by the green line in Fig. 14(a). Two sets of detuning frequencies and injection strengths can be found from the spectra of the free running SL and the ML. They are (15.471 GHz, 0.218) and (−38.689 GHz, 0.547). Fig. 15(b) shows the corresponding system output electrical spectrum. As shown, a dominant frequency component at 13.5 GHz was obtained, which demonstrates the

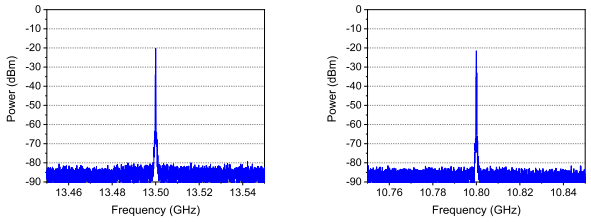

FIGURE 16. Output electrical spectra of the proposed 3/*N* frequency divider measured in a 100 MHz span when the SL forward bias current is adjusted to realise (a) 3/4 and (b) 3/5 frequency division. The ESA resolution bandwidth is 100 kHz and the ESA video bandwidth is 10 kHz.

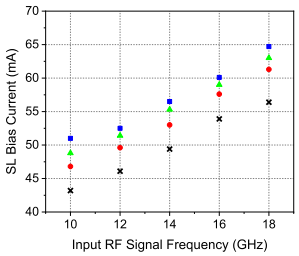

FIGURE 17. SL forward bias current required to realise 3/3 (black cross), 3/4 (red dot), 3/5 (green triangle) and 3/6 (blue square) frequency division versus the system input RF signal frequency.

3/4 frequency division operation since the input RF signal frequency is 18 GHz.

Fig. 15(a)-15(d) show the system output electrical spectra when the SL forward bias current was adjusted to obtain 2, 3, 4 and 5 optical frequency components between the regenerated -2^{nd} order and $+1^{st}$ order sidebands at the SL output. The measurements show, for an 18 GHz input RF signal, the system generates an 18 GHz, 13.5 GHz 10.8 GHz and 9 GHz output RF signal. This demonstrates a tunable 3/3, 3/4, 3/5 and 3/6 frequency division operation. Fig. 16 shows the system output spectra measured at around 13.5 GHz and 10.8 GHz when the SL forward bias current was adjusted to realise 3/4 and 3/5 frequency division respectively. This shows, as in the case of the 2/*N* frequency divider, the 3/*N* frequency divider has around 60 dB SNR in a 100 kHz noise bandwidth. The 3/*N* frequency divider with different frequency division ratios and different input RF signal frequencies of 10 to 18 GHz were experimentally demonstrated. The required SL forward bias currents to obtain different frequency division ratios for different input RF signal frequencies are shown in Fig. 17. A high SL forward bias current is needed to obtain a high frequency division ratio and to realise 3/*N* frequency division operation at a high input RF signal frequency.

V. CONCLUSION

Two microwave photonic signal processing structures for realising microwave frequency division with a tunable integer or non-integer division ratio have been presented. They are based on the optically injected semiconductor laser technique. They have simple and compact structures compared to the frequency dividers implemented by the regenerative or injection locking technique. The first structure, implemented by injecting a CS-DSB optical signal into a DFB laser, can realise 2/*N* frequency division. The second structure, implemented by injecting the -2^{nd} order and $+1^{st}$ order sidebands into a DFB laser, can realise 3/*N* frequency division. The frequency division ratio can be tuned by simply adjusting the DFB laser forward bias current. Simulation results have been presented to show the modulator extinction ratio, the FBG stopband rejection level, the coupler phase imbalance and the modulation index required to largely suppress the unwanted optical frequency components into the SL. Effects of the residual optical carrier into the SL in the 2/*N* frequency divider have been investigated experimentally. Methods have been proposed and demonstrated to ensure the unwanted frequency components at the system output are more than 27 dB below the frequency divided signal. 2/*N* and 3/*N* frequency divisions where *N* is between 3 to 6 have been verified experimentally. To our knowledge, this is the first report on realising 1/2, 1/3, 2/3 and 2/5 frequency division on a microwave photonic signal processing structure, and realising 1/2, 3/4 and 3/5 frequency division on another structure. Experimental results also show the proposed photonics-based microwave frequency dividers have stable and high SNR performance.

REFERENCES

[1] S. Duan, B. Mo, X. Wang, E. H. W. Chan, X. Feng, B. Guan, and J. Yao, "Photonic-assisted regenerative microwave frequency divider with a tunable division factor," *J. Lightw. Technol.*, vol. 38, no. 19, pp. 5509–5516, Oct. 1, 2020.

[2] Y. Chen, P. Zuo, T. Shi, and Y. Chen, "Photonic-based reconfigurable microwave frequency divider using two cascaded dual-parallel Mach–Zehnder modulators," *Opt. Exp.*, vol. 28, no. 21, pp. 30797–30809, 2020.

[3] S. Liu, K. Lv, J. Fu, L. Wu, W. Pan, and S. Pan, "Wideband microwave frequency division based on an optoelectronic oscillator," *IEEE Photon. Technol. Lett.*, vol. 31, no. 5, pp. 389–392, Mar. 1, 2019.

[4] Y. Xu, H. Peng, R. Guo, H. Du, Q. Yin, G. Hu, J. He, and Z. Chen, "Injection-locked millimeter wave frequency divider utilizing optoelectronic oscillator based optical frequency comb," *IEEE Photon. J.*, vol. 11, no. 3, pp. 1–8, Jun. 2019.

[5] Y. Meng, T. Hao, W. Li, N. Zhu, and M. Li, "Microwave photonic injection locking frequency divider based on a tunable optoelectronic oscillator," *Opt. Exp.*, vol. 29, no. 2, pp. 684–691, 2021.

[6] S.-C. Chan and J.-M. Liu, "Microwave frequency division and multiplication using an optically injected semiconductor laser," *IEEE J. Quantum Electron.*, vol. 41, no. 9, pp. 1142–1147, Sep. 2005.

[7] H. Chen and E. H. W. Chan, "Ultra-simple all-optical microwave frequency divider," *IEEE Photon. Technol. Lett.*, vol. 34, no. 4, pp. 219–222, Feb. 15, 2022.

[8] H. Chen and E. H. W. Chan, "Photonic microwave frequency divider with a tunable division ratio and harmonic suppression capability," *Opt. Exp.*, vol. 30, no. 19, pp. 34021–34033, 2022.

[9] T. Berceli and P. R. Herczfeld, "Microwave photonics—A historical perspective," *IEEE Trans. Microw. Theory Techn.*, vol. 58, no. 11, pp. 2992–3000, Nov. 2010.

[10] J. Capmany, J. Mora, I. Gasulla, J. Sancho, J. Lloret, and S. Sales, "Microwave photonic signal processing," *J. Lightw. Technol.*, vol. 31, no. 4, pp. 571–586, Feb. 15, 2013.

[11] R. Zheng, E. Chan, X. Wang, X. Feng, and B.-O. Guan, "Microwave photonic devices based on liquid crystal on silicon technology," *Appl. Sci.*, vol. 9, no. 2, p. 260, Jan. 2019.

[12] R. L. Miller, "Fractional-frequency generators utilizing regenerative modulation," *Proc. IRE*, vol. 27, no. 7, pp. 446–457, Jul. 1939.

[13] J. L. Li, S. W. Qu, and Q. Xue, "A theoretical and experimental study of injection-locked fractional frequency dividers," *IEEE Trans. Microw. Theory Techn.*, vol. 56, no. 11, pp. 2399–2408, Nov. 2008.
[14] T. H. Cheung, J. Ryynänen, A. Pärssinen, and K. Stadius, "A 5.4-GHz 2/3/4-modulus fractional frequency divider circuit in 28-nm CMOS," in *Proc. IEEE Int. Symp. Circuits Syst. (ISCAS)*, May 2021, pp. 1–5.
[15] L. Fan, Z. M. Wu, T. Deng, J. G. Wu, X. Tang, J. J. Chen, S. Mao, and G. Q. Xia, "Subharmonic microwave modulation stabilization of tunable photonic microwave generated by period-one nonlinear dynamics of an optically injected semiconductor laser," *J. Lightw. Technol.*, vol. 32, no. 23, pp. 4660–4666, Dec. 1, 2014.
[16] X.-Q. Qi and J.-M. Liu, "Photonic microwave applications of the dynamics of semiconductor lasers," *IEEE J. Sel. Topics Quantum Electron.*, vol. 17, no. 5, pp. 1198–1211, Sep. 2011.
[17] Y. H. Hung and S. K. Hwang, "Photonic microwave stabilization for period-one nonlinear dynamics of semiconductor lasers using optical modulation sideband injection locking," *Opt. Exp.*, vol. 23, no. 5, pp. 6520–6532, 2015.
[18] S.-K. Hwang, J.-M. Liu, and J. K. White, "Characteristics of period-one oscillations in semiconductor lasers subject to optical injection," *IEEE J. Sel. Topics Quantum Electron.*, vol. 10, no. 5, pp. 974–981, Sep. 2004.
[19] S.-C. Chan, S.-K. Hwang, and J.-M. Liu, "Period-one oscillation for photonic microwave transmission using an optically injected semiconductor laser," *Opt. Exp.*, vol. 15, no. 22, pp. 14921–14935, Oct. 2007.
[20] C. Wang, M. Zhang, X. Chen, M. Bertrand, A. S. Ansari, S. Chandrasekhar, P. Winzer, and M. Loncar, "100-GHz low voltage integrated lithium niobate modulators," in *Proc. Conf. Lasers Electro-Opt. (CLEO)*, May 2018, pp. 1–2, Paper SM3B.4.
[21] (2020). *DWDM Fiber Bragg Gratings (12.5/25/50/100/200 Hz) Datasheet*. [Online]. Available: http://www.o-eland.com/FiberGratingProducts/OEWDM.pdf
[22] (2019). *Marki Microwave 3 dB Quadrature Hybrid (QH-0440) Datasheet*. [Online]. Available: http://www.markimicrowave.com
[23] H. Kiuchi, T. Kawanishi, M. Yamada, T. Sakamoto, M. Tsuchiya, J. Amagai, and M. Izutsu, "High extinction ratio Mach–Zehnder modulator applied to a highly stable optical signal generator," *IEEE Trans. Microw. Theory Techn.*, vol. 55, no. 9, pp. 1964–1972, Sep. 2007.
[24] H. Chen and E. H. W. Chan, "Wideband photonic microwave frequency divider with large harmonic suppression capability," *IEEE Photon. J.*, vol. 14, no. 4, pp. 1–8, Aug. 2022.

HAO CHEN (Member, IEEE) received the B.E. degree in electronic information science and technology from the Tianjin University of Technology, Tianjin, China, in 2006, and the M.E. degree in electrical and electronics engineering from Charles Darwin University, Australia, in 2016, where he is currently pursuing the Ph.D. degree. His research interests include microwave photonic signal processing, which includes frequency mixers, angle of arrival measurement, and frequency dividers.

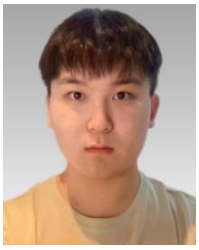

MINGTONG LIU received the B.E. degree in electrical engineering and automation from Yanshan University, China, in 2019, and the M.E. degree in electrical and electronics engineering from Charles Darwin University, Australia, in 2022. His research interests include microwave photonic signal processing, and frequency and angle of arrival measurement.

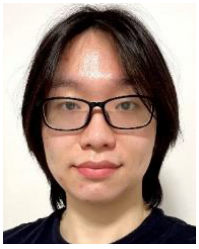

AOQI LI received the B.E. degree in integrated circuit design and integrated systems from the Dalian University of Technology, China, in 2020, and the M.E. degree in electrical and electronics engineering from Charles Darwin University, Australia, in 2022. His research interests include photonic microwave measurement and sensing.

ERWIN H. W. CHAN (Senior Member, IEEE) received the B.Sc., B.Eng. (Hons.), and Ph.D. degrees from The University of Sydney, Australia, in 1998, 2000, and 2005, respectively.

He was a Senior Research Fellow and an External Lecturer with The University of Sydney, from 2005 to 2014. He is currently an Associate Professor with the College of Engineering, IT and Environment, Charles Darwin University, Australia. He has published more than 160 papers in international refereed journals and conferences, and has carried out consulting work with industry. His research interests include microwave photonics, optical telecommunications, optical signal processing, and photonic and microwave technology.

Dr. Chan has been a member of the Technical Program Committee of the Conference on Laser and Electro-Optics (CLEO). He was a recipient of the University of Sydney Early Career Development Award and the Australian Postdoctoral Fellowship from the Australian Research Council.